

School of Natural Sciences and Mathematics

***AVA Analysis and Interpretation of a Carbonate
Reservoir: Northwest Java Basin, Indonesia***

UT Dallas Author(s):

Adriansyah
G. A. McMechan

Rights:

©2001 Society of Exploration Geophysicists. All rights reserved.

Citation:

Adriansyah and G. A. McMechan. 2017. "AVA analysis and interpretation of a carbonate reservoir: Northwest Java basin, Indonesia." *Geophysics* 66(3), doi:10.1190/1.1444964

This document is being made freely available by the Eugene McDermott Library of the University of Texas at Dallas with permission of the copyright owner. All rights are reserved under United States copyright law unless specified otherwise.

AVA analysis and interpretation of a carbonate reservoir: northwest Java basin, Indonesia

Adriansyah* and George A. McMechan[†]

ABSTRACT

A detailed analysis is performed of amplitude variation with angle (AVA) observations in six common-midpoint gathers with reflection points that are over and beside carbonate reefs in the Parigi Formation in the northwest Java basin. Both empirical analysis and full-wavefield modeling of the AVA data suggest that the presence of gas affects AVA by reducing the bulk density of the reservoir, decreasing of the overburden V_p/V_s ratio and by local attenuation caused by gas sieving through the overlying sediments. The slopes of AVA curves for reflections from the top of the Parigi are negative for brine saturation and strongly positive for gas saturation.

INTRODUCTION

In 1955, Koefoed published a set of curves showing the variation of reflection coefficient with angle of incidence for a plane wave for interfaces with various contrasts in Poisson's ratio. This led to the development of the amplitude variation with offset (AVO) approach for interpreting seismic amplitude anomalies in terms of lithology and fluid content (e.g., Ostrander, 1984; Shuey, 1985; Rutherford and Williams, 1989). Poisson's ratio is dependent on the lithology and fluids present in a reservoir (Gregory, 1976).

Even though many factors affect reflection amplitude observations (e.g., Samec and Blangy, 1992; Juhlin and Young, 1993; Kim et al., 1993; Martinez, 1993; Xu et al., 1993; Widmaier et al., 1996), AVO has proven useful in hydrocarbon exploration, especially for shallow gas-sand reservoirs in clastic environments such as the Texas Gulf Coast (Allen and Peddy, 1993; Estill and Wroldstad, 1993; Hall et al., 1995), the Arabian Gulf (Chiburis, 1984, 1993), and the North Sea (Snyder and Wroldstad, 1992; Landrø et al., 1995). In contrast, there are only a few reported examples of AVO applications to exploration in carbonates (Chiburis, 1987, 1993; Lu and Lines, 1995).

Chacko (1989), Santoso et al. (1995), Piggot et al. (1990), Ho et al. (1992), and D'Angelo et al. (1997) report successful application of AVO techniques in carbonate exploration.

The main exploration problem for carbonate reservoirs in the northwest Java basin is determining the porosity distribution within reefs. Santoso et al. (1995) estimated the porosity of a carbonate reservoir in the basin using an inversion technique. Chacko (1989) successfully distinguished between tight and porous limestones using AVO signatures in south Sumatra, whose geology is similar to the northwest Java basin. In this study, we extract, simulate, and analyze the angle-dependent responses of interfaces between the lower Cisubuh (shale) and Parigi (carbonate) Formations in the northwest Java basin to predict the distribution of porosity and the presence of gas in the upper part of the carbonate reservoir.

GEOLOGIC SETTING

The study area is the northwest Java basin in Indonesia, located both offshore and onshore at the southernmost edge of the continental Sunda plate (Figure 1). The present basin area was formed by continuous subsidence and southward tilting of the Sunda plate since the Early Tertiary (Hamilton, 1976). The basin consists of several subbasins separated by high areas. Hydrocarbons are produced from various types of reservoirs (Reminton and Pranyoto, 1985), including volcanic clastics (the Jatibarang Formation), sandstone and limestone clastics (the Cibulakan Member), and reef carbonates (the Parigi and Cibulakan Formations). The data used in the study presented below are from one of the hydrocarbon fields located between the Pasir Putih and the Jatibarang subbasins. North-south-trending block faults dominate the basin structure (Patmosukismo and Yahya, 1974) and provide good migration paths for hydrocarbons generated in the Talang Akar Shale of the Cibulakan Member (Yaman et al., 1991; Arianto, 1993). Another hydrocarbon migration mechanism in this region is capillary sieving (Arianto, 1993).

The target layer is the Parigi Formation, one of the main hydrocarbon producers in the northwest Java basin, especially

Manuscript received by the Editor December 28, 1998; revised manuscript received June 29, 2000.

*University of Texas at Dallas, Center for Lithospheric Studies, P.O. Box 830688, Richardson, TX 75083-0688, and Pertamina Indonesia, Exploration Division, Jl. Merdeka Timur 6, Jakarta 10110, Indonesia.

[†]University of Texas at Dallas, Center for Lithospheric Studies, P.O. Box 830688, Richardson, TX 75083-0688. E-mail: mcmec@utdallas.edu.

© 2001 Society of Exploration Geophysicists. All rights reserved.

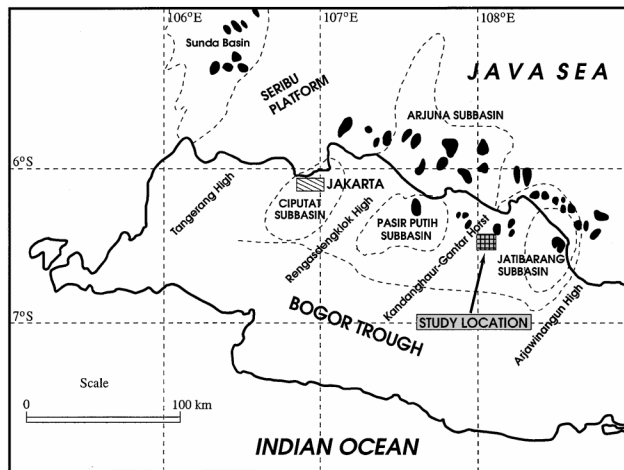


FIG. 1. The Northwest Java Basin. The data for this study come from an area located between the Jatibarang and the Pasir Putih subbasins. The dashed lines outline the subbasins. Black areas are known oil and gas fields.

in the Jatibarang and Arjuna subbasins. The Parigi Formation is composed of limestone with minor local dolomitic and sandy limestone, with thickness ranging from 27 to 450 m. The Parigi and pre-Parigi carbonate buildups are excellent targets for gas exploration because of their high productivity and abundance and because drilling/development costs are low as they occur at relatively shallow depth. Stratigraphically, the Parigi buildup is positioned between the pre-Parigi (upper Cibulakan) and Cisubuh Formations (Figure 2) that were deposited in a shallow marine environment during regional tectonic quiescence in the late Miocene (Burbury, 1977; Santoso et al., 1995). Yaman et al. (1991) divide the Parigi into three subdivisions: a thin (6–9 m) lower Parigi basal unit overlain by a thicker (12–30 m) middle Parigi claystone unit, which in turn is overlain by the upper Parigi unit, an excellent gas reservoir.

High average porosity (30%) and permeability (>2 darcies) of the Parigi are documented by Yaman et al. (1991) and Santoso et al. (1995). The microporosity in the carbonate (Wight and Hardian, 1982; Yaman et al., 1991) is enhanced by moldic and vugular pores developed by both early- and

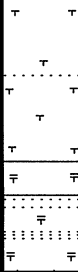
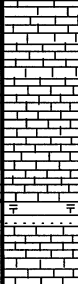
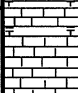


AGE		FORMATION	LITHOLOGY	DEPTH (M)	OIL SHOWS	RESERVOIR INFORMATION		
RECENT TO PIOCENE		C I S U B U H		500		<p>Parigi Formation:</p> <p>Good reefal carbonate reservoirs sealed by the mudstones of the Cisubuh Formation. Oil and gas are produced from the Parigi in the Jatibarang subbasin.</p> <p>Upper Cibulakan Member:</p> <p>The organic carbon content is below average, but thin coals with minor oil and gas potential occur. The fine sandstone and limestones in the lower part are good reservoirs sealed by Middle Miocene mudstones. Some of the main producing reservoirs in the Arjuna and Jatibarang subbasin.</p> <p>Middle Cibulakan Member:</p> <p>Dominantly shallow marine limestone with no source rock potential. Good reefal reservoirs, with seals provide by the Upper Cibulakan Member. One of the main producing reservoirs in the Northwest Java basin.</p> <p>Lower Cibulakan Member:</p> <p>A good to very good source rock. The quality and thickness increase toward the dipocenter of subbasin. Oil and gas are produced from sandstone reservoirs. Seals are provided by Lower Cibulakan mudstones.</p>		
MIOCENE				PARIGI				1000
UPPER								UPPER CIBULAKAN
MIDDLE		ZONE - 16						
LOWER				BATURAJA				
OLIGOCENE							2000	

FIG. 2. Stratigraphic column for the northwest Java basin derived from well PCT-1. Well location is shown in Figure 3. After Burbury (1977).

late-stage dissolution (by meteoric diagenesis) leading to the high effective permeability.

The exploration well PCT-1 (Figure 3) was drilled in 1992 to 2300 m depth to investigate hydrocarbon-bearing zones in

the Parigi, zone 16 (equivalent to the middle Cibulakan), the Baturaja (equivalent to the lower Cibulakan), and the underlying volcanic Jatibarang Formation. The Parigi was encountered at 965 m depth (Figure 2) and consists of 370 m of wackestone-packstone and packstone-grainstone limestones. The overlying lower part of the Cisubuh Formation consists of shale and low-porosity sandstone. Hydrocarbon tests in the Parigi Formation indicated a noneconomic oil show.

WELL-LOG DATA

Figure 4 shows the P -wave sonic, density, and gamma logs measured from well PCT-1. Notice the sharp increase of both P -wave velocity (V_p) and density (ρ) at the top of the target (Parigi) limestones at 965 m depth. This large contrast gives a high-amplitude reflection at ~ 1.1 s with good S/N ratio and so is amenable to AVO analysis. To analyze this boundary in more detail, Figure 5 shows the crossplot of the V_p and ρ values from the logs in Figure 4 with the corresponding least-squares second-order (solid) curve that fits the Parigi observations. The uppermost ~ 40 m of the Parigi has higher ρ than its central region; Figure 5 (the red points) suggests this may be caused by a high shale content right at the top of the Parigi, which is consistent with the locally high gamma values (Figure 4c). Similarly, the increase in density (Figure 4b) and gamma (Figure 4c) with depth at the bottom of the Parigi may also be interpreted as increasing shale content (the green points, Figure 5). For the purpose of synthetic seismogram modeling, the V_p - ρ relation for clastics published by Gardner et al. (1974) was used to predict the density profile at depths < 880 m and > 1340 m, where no density logs were recorded.

SEISMIC DATA PROCESSING

The northwest-southeast-trending seismic line GT-8 (Figure 3) lies almost perpendicular to the Parigi depositional strike (Burbury, 1977; Yaman et al., 1991) and goes through well PCT-1 at shotpoint 300. Data were acquired on this line by Compagnie Générale de Géophysique using an SN235 seismic

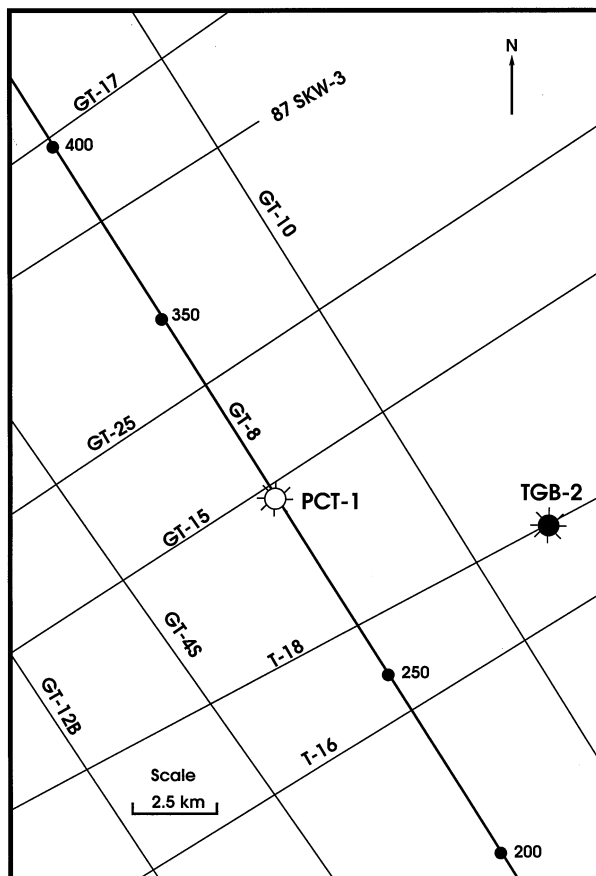


FIG. 3. Base map for seismic line GT-8. Numbers along line GT-8 are shotpoints. Well PCT-1 is located at shotpoint 300. Other labeled lines are seismic surveys not used in this study.

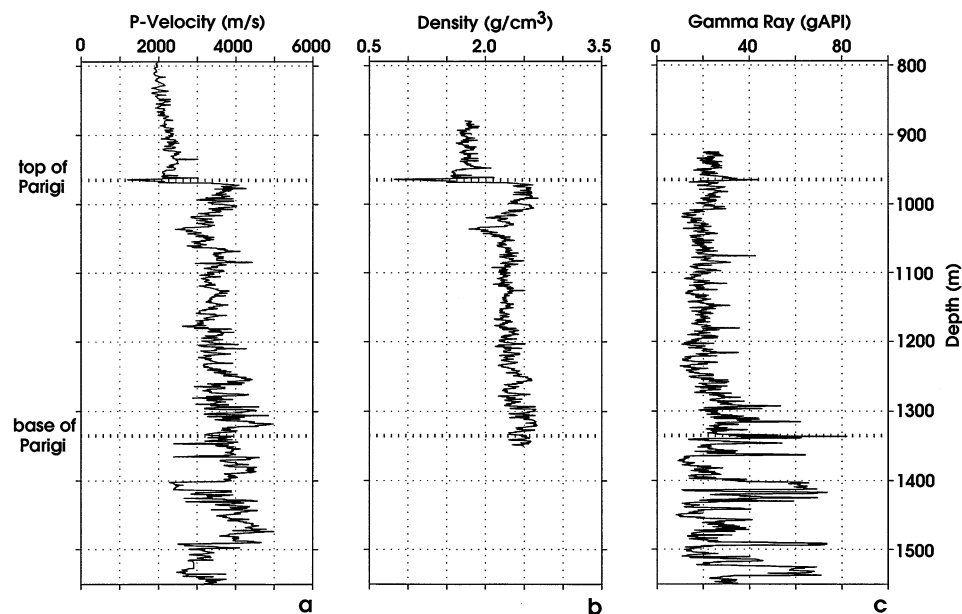


FIG. 4. (a) Sonic, (b) density, and (c) gamma logs from well PCT-1. Data are plotted only for depth ranges for which logs were obtained.

system. The record length is 5 s with a 4-ms sample interval. Each shotpoint has 24 traces with a 60-m geophone group interval. Dynamite sources were used, with a 120-m interval between shotpoints. The nearest offset receiver is at 480 m. Shooting was off-end. The field data were obtained with no processing applied (no deconvolution, amplitude balancing, or filtering), so we had tight control on the amplitudes throughout our analysis. The only factor we do not have information on

is the filtering performed by the geophone groups during acquisition. Since these were designed to discriminate against ground roll, they should have only a minor effect on the reflections of interest here.

The stacked section of line GT-8 is shown in Figure 6. The top of the Parigi Formation is the strong reflection that varies from 1.1 to 1.5 s two-way traveltime. Two reef buildups are distinguished in the seismic section, between shotpoints 100–180 and 250–350. Six common-midpoint (CMP) gathers located at the marked positions in Figure 6 were selected for amplitude variation with angle (AVA) analysis and are individually plotted in Figure 7. Well PCT-1 is located at CMP 3. These CMPs represent various aspects of the reef environment at locations where the Parigi reflections are nearly flat, so dip corrections were not needed.

Each actual CMP has a maximum of only six offsets. Each CMP supergather in Figure 7 was constructed by combining traces from 50 CMP gathers centered around each of the CMP locations shown in Figure 6 to obtain 24 offsets in each CMP. This CMP window was chosen because it corresponds to stable (very similar) relative times and amplitudes of the Parigi reflection at any offset within the window, so the traces at each offset could be vertically stacked with little distortion to enhance the S/N ratio. The CMP gathers (Figure 7) show that amplitudes generally decrease with incident angle (with increasing offset), with the exception of CMP 4, in which amplitudes increase with angle. This anomalous behavior is analyzed below.

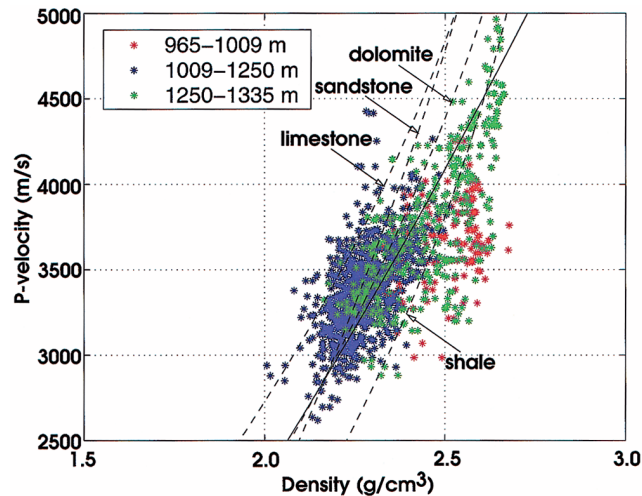


FIG. 5. Crossplot of P -wave velocity and density-log data from the carbonate (Parigi) portion of well PCT-1. The solid line is the least-squares second-order curve fitted to the data. For comparison, the dashed lines are curves for limestone, dolomite, sandstone, and shale as published by Castagna et al. (1993).

Velocity analysis

The semblance plots of the velocity analysis for the six CMP gathers in Figure 7 are shown in Figure 8. The uncertainty

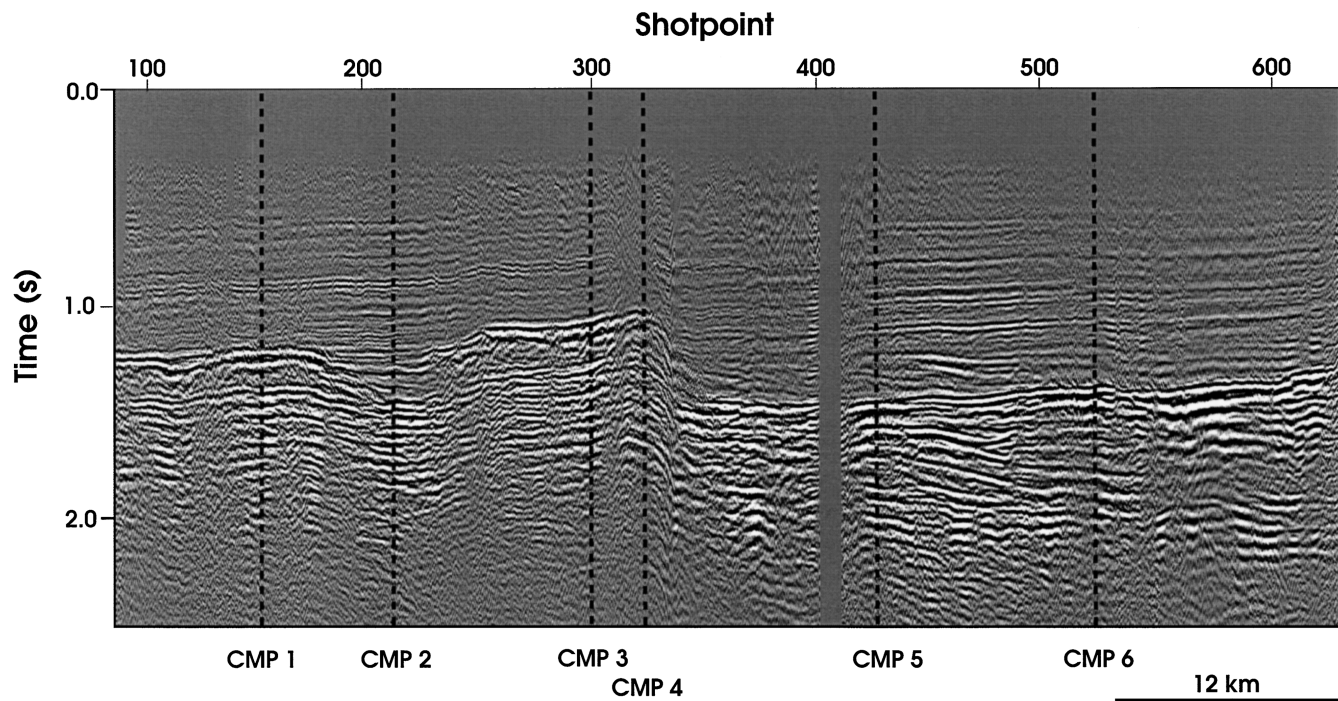


FIG. 6. Stacked seismic section of line GT-8. Six CMPs (from the locations labeled 1 through 6) are analyzed. For scale, there are 100 shotpoints in 12 km.

in these estimates is indicated by the width of the images ($\sim \pm 100$ m/s). For the CMPs that sample the reefs, a sharp increase of stacking velocity occurs at times corresponding to the top of the Parigi horizon in Figure 6 (1.2, 1.1, and 1.0 s for CMPs 1, 3, and 4, respectively). CMPs 2, 5, and 6 also contain high-amplitude reflections from Parigi strata, but these are at off-reef locations. CMP 2 corresponds to an interreef lagoon position, and CMPs 5 and 6 show basin features seaward of the reefs (Figure 6); these Parigi reflections are probably from the platform on which the reef was deposited, covered by reef talus and other clastic sediments that are of lower velocity than that of the carbonates in the reef cores (Table 1).

Figure 9 shows three interval velocity profiles at well PCT-1 (at CMP 3). These are from the sonic log, the seismic velocity analyses (Figure 8), and a blocked version of the sonic log used

below for synthetic seismogram synthesis. Higher overburden velocities are predicted by the seismic data (the dashed line) than by the sonic log (the solid line). As a consequence, the depth of the Parigi predicted by the seismic data is deeper than that observed in the well. The zero-offset two-way reflection traveltimes from the surface down to the top of the Parigi are the same for both models. However, the corresponding reflection-time moveouts are very different: that from the analysis of seismic (CMP 3) data fits the field data, whereas the times predicted by the well-log model deviate progressively to later times as offset increases. This suggests the presence of anisotropy in the overburden.

By forcing the Parigi reflection to occur at its known depth (965 m), the amount of anisotropy in the overburden can be estimated from the observed nonhyperbolic moveout by fitting

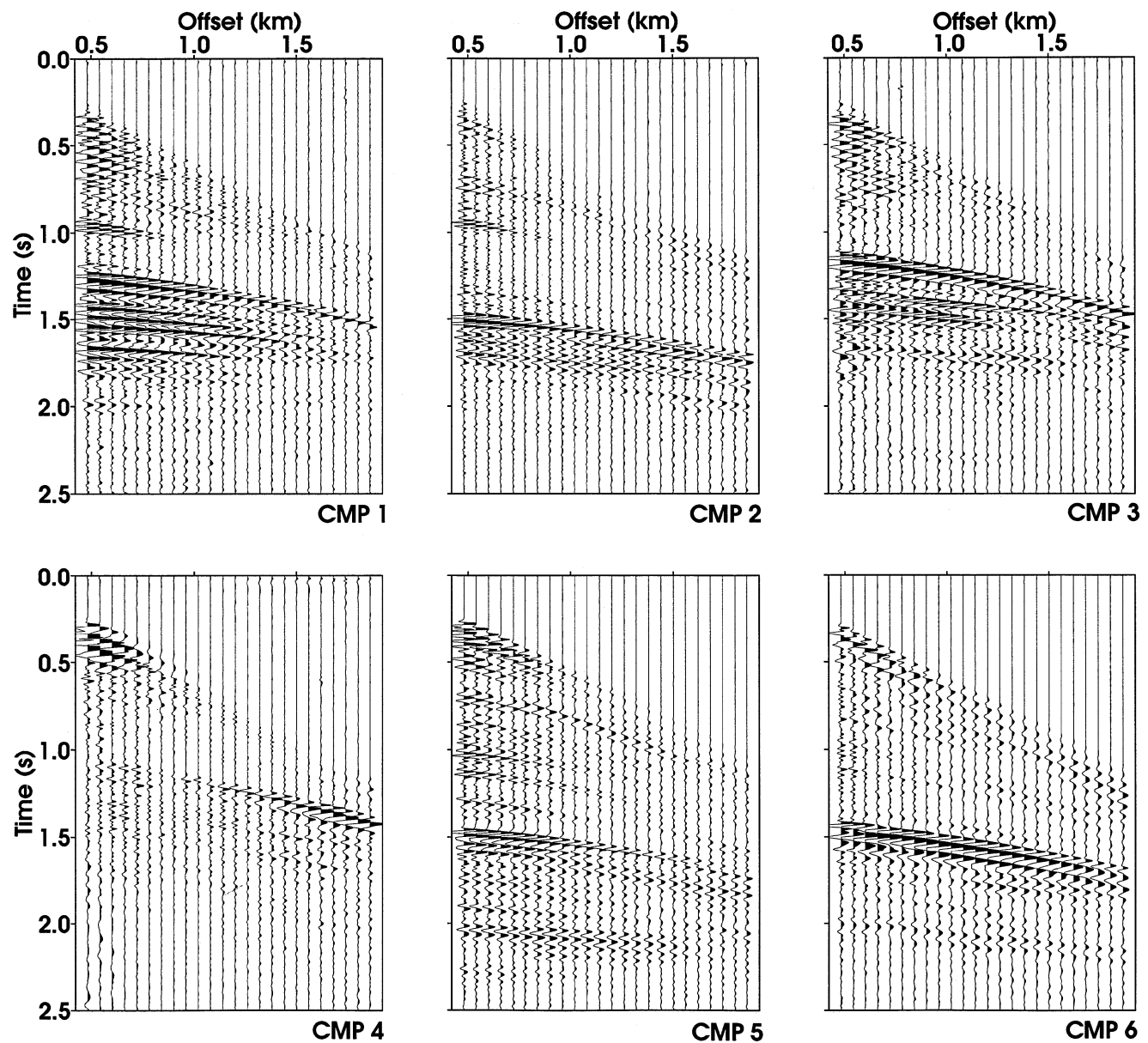


FIG. 7. Raw plots of the six CMP gathers labeled in Figure 6. At the target depth (1.1 to 1.5 s), CMPs 1, 3, and 4 sample reefs; CMPs 2, 5, and 6 sample carbonate between or beside the reefs.

the moveout data using the transversely isotropic formula of Hake et al. (1984) and Alkhalifah (1997):

$$t^2(X) = t_0^2 + \frac{X^2}{V_{\text{nmo}}^2} - \frac{2\eta}{t_0^2 V_{\text{nmo}}^4} X^4, \quad (1)$$

where $t(X)$ is the two-way reflection time at offset X , t_0 is the zero-offset reflection time, and η is the anisotropy parameter

that relates the NMO P -wave velocity (V_{NMO}), (which is the effective vertical P -wave velocity) with the horizontal P -wave velocity (V_h) denoted by

$$V_h = V_{\text{nmo}} \sqrt{1 + 2\eta}. \quad (2)$$

Assuming the amount of anisotropy is constant with depth through the overburden, we get $\eta = 0.049145$ and

Table 1. Elastic model parameters for the Cisubuh overburden and the Parigi targets. Interval P -wave velocities were obtained from the seismic velocity analyses shown in Figure 8. The overburden S -wave velocity and density are calculated using the relations given by Castagna et al. (1993) and by Gardner et al. (1974). For the target, the S -wave velocity is obtained from iterative AVA curve fitting. These parameters are then used to calculate responses shown in Figures 10 and 11.

	Value	CMP 1	CMP 2	CMP 3	CMP 4	CMP 5	CMP 6
Overburden	V_p (m/s)	2580	2354	2311	2149	2292	2190
	V_s (m/s)	1119	945	912	1343	897	819
	Density (g/cm ³)	2.207	2.157	2.147	2.108	2.143	2.118
	V_p/V_s	2.31	2.48	2.53	1.6	2.56	2.67
Target	V_p (m/s)	4044	3143	3609	3465	2991	2887
	V_s (m/s)	2450	1654	2062	1873	1869	1520
	Density (g/cm ³)	2.483	2.247	2.374	1.950	2.204	2.174
	V_p/V_s	1.65	1.90	1.75	1.85	1.60	1.90

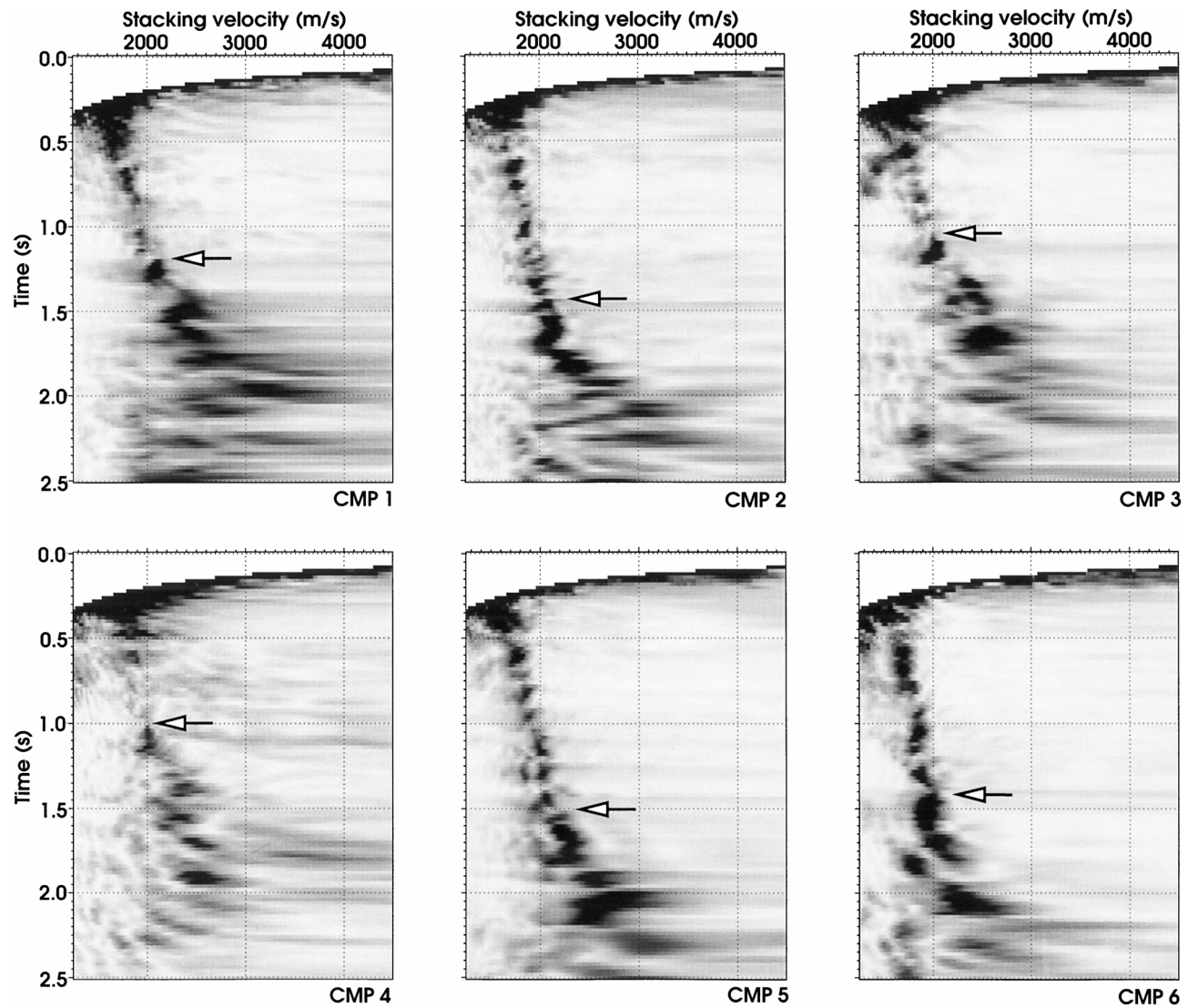


FIG. 8. Semblance velocity plots for each CMP in Figure 7. Arrows indicate the top of the Parigi.

$V_h/V_{\text{vmo}} = 1.048$, which corresponds to 4.8% anisotropy. The horizontal velocity is faster than the vertical, as expected in a layered sand/shale sequence. Numerical simulation of the observations using this overburden anisotropy incorporates its effects into the resulting synthetic AVA curves.

SEISMIC DATA ANALYSIS

Model building and AVA analysis

The goal of amplitude analysis is to find a model that reasonably reproduces the seismic amplitude observations and that is sufficiently well constrained by the geologic environment that it generates geologically plausible explanations. In the present context, we use an elastic parameterization consisting of P - and S -wave velocities and density (V_p , V_s , and ρ , respectively). We need to develop a set of related models that fits all of the six representative CMPs (Figure 7) simultaneously.

Table 1 shows the seismic models obtained for the Cisubuh/Parigi interface for each of the six CMP locations. For each model, the V_p values used were obtained from the velocity analysis described above. The ρ values used were predicted from the V_p values (except for CMP 3, where a log was available), using the least-squares fit (solid) curve in the $V_p - \rho$ crossplot (Figure 5) for the carbonate and the $V_p - \rho$ relation of Gardner et al. (1974) for the clastic section. [The former is very similar to the curve presented by Castagna et al. (1993)

for dolomite.] Thus, the models are consistent with those found for similar lithologies at other sites.

No S -wave velocity (V_s) information was available. In the Cisubuh overburden, which consists of shale, sandstone, and mudstone, the shear-wave velocity can be predicted confidently using the relation published by Castagna et al. (1993), as these lithologies all behave similarly in terms of V_p/V_s ratio. Chacko (1989) concludes that, for many carbonates, a V_p/V_s ratio of 1.9 (as observed in the Alberta basin) is nearly invariant with respect to porosity. This observation is also reported by Santoso et al. (1995) for the Parigi carbonate. However, for low-velocity carbonate, the V_p/V_s ratio can reach as high as 2.8 (Anselmetti and Eberli, 1993), and significantly lower-than-average V_p/V_s ratios can be the result of dolomitization (e.g., Schlumberger, 1984). Thus, the V_p/V_s ratio for the target at each CMP was estimated by a two-step iterative procedure. First, an approximate V_s value was defined as that which best reproduced the AVA behavior when combined with the V_p and ρ values in the elastic Zoeppritz (1919) reflection coefficients for the P -wave reflections. To do this, the field-data amplitudes were corrected for spherical divergence and for the incidence angle at the receiver (to get total amplitude from the vertical component) prior to amplitude picking. The second step involved fine-tuning by the full-wave model described below.

The amplitude scale factors that produce the best match between the field and predicted data for each CMP (for both the AVA in this section and the synthetic CMP gathers in the next section) differ only a maximum of 17% across all six CMP gathers. This internal consistency across gathers adds to the confidence that the scaling is reasonable and allows comparisons between AVA curves.

Synthetic seismogram modeling

Figure 10 shows the real and synthetic traces in 200-ms windows around the target reflection for each of the six CMPs, after offset-dependent shifting to produce flattening in time. No

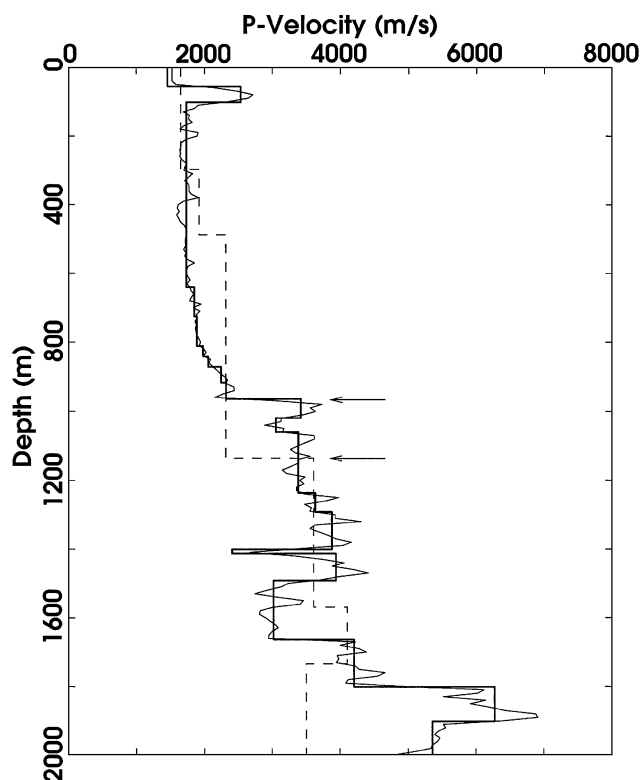


FIG. 9. Interval velocity profiles at well PCT-1 (CMP 3). The light solid curve is the velocity obtained from the sonic log. The heavy solid curve is the blocked average log velocity. The dashed line is the velocity profile obtained by velocity analysis of CMP 3. The deeper prediction of the target depth (at the arrows) by the seismic analysis is because of the higher apparent overburden interval velocities associated with anisotropy.

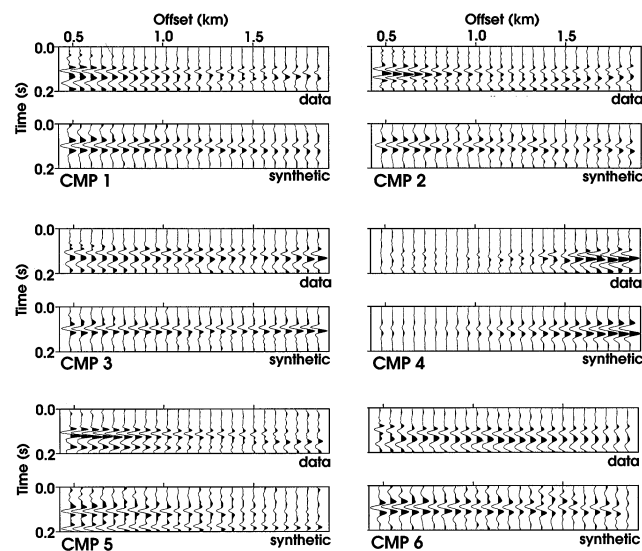


FIG. 10. Traces for the six CMP gathers in Figure 7 and the corresponding synthetic responses, after flattening around the Parigi reflection time and extracting 200-ms windows. CMP locations are shown in Figure 6.

NMO correction was applied to preserve the original wavelet shape and amplitude. The field-data wavelet seems visually to be fairly constant in shape from CMP to CMP (Figure 7), which facilitates consistency in amplitude picking for AVA analysis. Amplitudes used were peak-to-trough measurements to reduce dependence on the wavelet shape.

The 1.5-D τ - p domain reflectivity modeling technique developed by Martinez and McMechan (1991) is modified and used to calculate the synthetics (except for CMP 4, which required finite differences to model a low Q gas chimney, as described below). The source function is a zero-phase Ricker wavelet with a dominant frequency of 35 Hz. The models are elastic (except for CMP 4) and contain a transversely isotropic overburden with 4.8% anisotropy (as calculated above). Transmission losses are automatically included in the modeling. The model values for the target/overburden interface are given in Table 1.

The traces in Figure 10 are plotted with positive impedance contrast as a trough. There was no attempt to shape the observed wavelet through deconvolution because of the lack of explicit source wavelet information. Nevertheless, the synthetic relative amplitude data appear to fit well with the field data. The observed and final synthetic AVA curves are shown in Figure 11. The observed AVA curves were smoothed to reduce the measurement variance.

The off-reef CMP locations (2, 5, and 6) for which the AVA curves decrease almost monotonically (Figure 11) are synthesized reasonably well, especially at CMP 5. The responses of CMPs 2 and 6 at angles greater than 15° , are consistent with Pickett's relation (Pickett, 1963; Chacko, 1989; Castagna et al., 1993) of $V_p/V_s = 1.9$ (Table 1). In the AVA responses at small angles of incidence ($<15^\circ$), the observed field-data amplitudes are higher than predicted in CMP 2 and lower than predicted in

CMP 6. These differences could be produced by the local focusing and defocusing (Adriansyah and McMechan, 1998) in the near-surface velocity structure or by interference of converted waves and/or interbedded multiples originating at shallower depths with the primary Parigi reflections.

The observed and predicted responses for the on-reef CMPs 1 and 3 show a typical AVA response of a carbonate reservoir overlain by lower velocity sediment (e.g., Richards, 1961; Chacko, 1989; Dey-Sarkar and Svatek, 1993), in which the zero-offset reflectivity is high and the trend is affected by a critical reflection whose influence (as a positive AVA slope) begins to occur at a relatively small incidence angle of about 35° – 40° . The AVA response of CMP 3 fits reasonably with a carbonate V_p/V_s ratio of 1.75, especially at intermediate angles of incidence, while the AVA response of CMP 1 beyond 15° incidence angle varies around the predicted response for $V_p/V_s = 1.65$. We know from the well at CMP 3 that the reservoir is brine saturated (with only a trace of oil) at this location.

Gas saturation at CMP 4

The response of CMP 4 (Figure 10) is clearly anomalous; it is nowhere near any of the other AVA curves. The AVA at CMP 4 has low near-offset amplitudes and a steeply increasing amplitude beyond 1200 m offset, which is opposite to all the other CMPs (Figure 10). This behavior is qualitatively consistent with the hypothesis that the upper Parigi at CMP 4 is gas saturated and that this gas also sieves into the overlying sediments; we now (1) examine what other evidence exists for this interpretation and (2) build and test the corresponding model.

We began by treating CMP 4 the same as all the others. This involved keeping the V_p/V_s ratio in the carbonate near

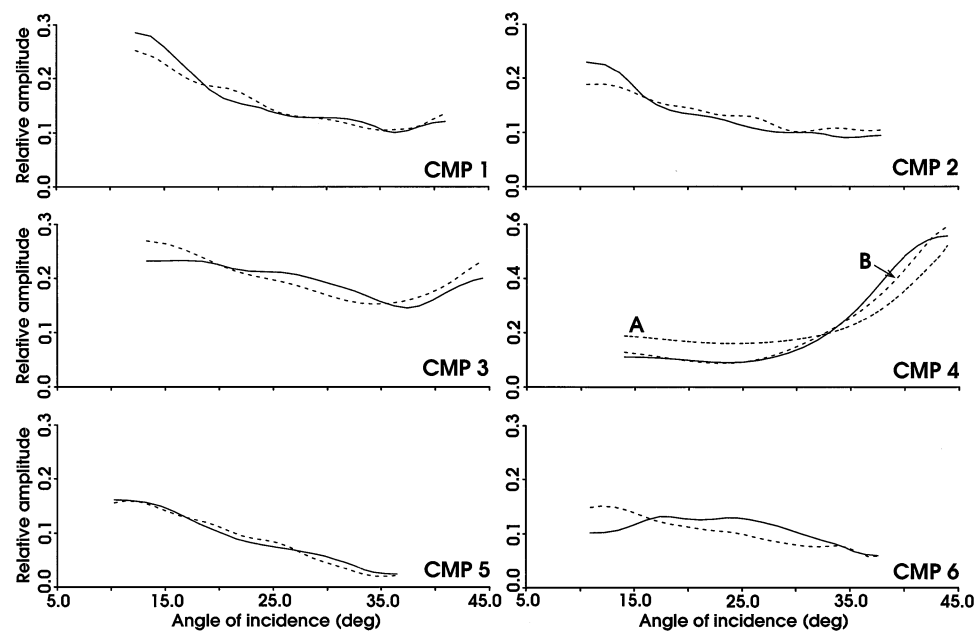


FIG. 11. AVA responses picked from the windowed traces in Figure 10. The heavy solid lines are for the field data, and the dashed lines are for the synthetic data. The vertical (relative amplitude) scale for CMP 4 is twice that of the others. For CMP 4, curve A is the prediction of the elastic model and curve B is the prediction of the viscoelastic model, which includes a low- Q , vertically oriented gas zone in the sediment above the reservoir.

to 1.9 (Chacko, 1989), using published empirical relations to predict V_s and ρ in the overburden, and using the solid line in Figure 5 to predict ρ in the Parigi. The latter was then reduced (to 1.95 g/cm³), assuming 35% porosity (see next section) and full gas saturation at the top of the Parigi. The AVA response of this model is shown as curve A in the CMP 4 panel in Figure 11; it approximately predicts the observed fairly flat AVA at incident angles $<30^\circ$ and the steep amplitude gradient at angles $>30^\circ$. However the near-offset amplitudes are too high by a factor of ~ 2 and the amplitude gradient is too low between 20° and 40° .

The key to constructing the final model is in the stacked seismic section (Figure 6); the reflections from the whole sediment column above the Parigi (as well as the Parigi reflection) in the neighborhood of CMP 4 are all locally attenuated. This behavior is consistent with low P -wave Q values caused by sieving gas from the Parigi reservoir into the overlying sediments. [A locally dim stack is also consistent with the polarity changes in a Type I AVO response (Rutherford and Williams, 1989) for a high-impedance sand beneath a shale. This would not, however, affect the reflections within the overlying sediment as we see here (Figure 6) and is inconsistent with the AVA behavior seen in Figures 10 and 11.]

To simulate the response of the gas chimney, we reduce the V_p/V_s of the overlying sediment to 1.6 by locally decreasing V_p and increasing V_s , consistent with the density decrease. We also inserted a low Q [$Q_p = 15$, $Q_s = 25$, which is consistent with $Q_s/Q_p < 1$ in gas sand (Klimentos, 1995)] centered on CMP 4 (at the topographic high of the reef). This zone increased in width from ~ 100 m at the top of the Parigi to ~ 900 m near the surface and was tapered at its lateral edges to simulate lateral diffusion of the gas. The low Q zone produces maximum attenuation at the near offset and decreases nonlinearly to near zero attenuation at the farther offsets. Superimposing this effect onto the nonattenuating model produces the final AVA fit for CMP 4, shown as curve B in the CMP 4 panel in Figure 11. Including the gas chimney attenuation has the desired effects of reducing the amplitudes at incident angles $<30^\circ$ and increasing the amplitude gradient between 25° and 40° . The amplitude behavior at the adjacent CMPs is also consistent with this model. Two other scenarios that also produce similar AVA fits without the attenuation contain a 23° dip of the top of the Parigi or a -9.8% anisotropy in the overburden (i.e., a vertical velocity 9.8% faster than the horizontal velocity); neither of these makes geologic sense. The elastic properties of the final model are given in Table 1.

The gas model for CMP 4 is thus supported by two separate pieces of information. These are the requirement of low V_p/V_s in the sediment (to get an increasing AVA response) and the observed high attenuation in the interpreted gas chimney (that produces the final AVA fit).

Porosity estimation from elastic seismic parameters

Porosity prediction of carbonate reservoirs from AVA observations can be done by modeling (Chacko, 1989) or by direct calculation using seismic parameters obtained by AVA analysis as in the previous section (Piggot et al., 1990; Santoso et al., 1995). If the lithology is known, one can predict the porosity directly from density; porosity can also be predicted from P - and S -wave velocity or Poisson's ratio (e.g., Domenico, 1984, 1993) using the time-average equation (Wyllie et al., 1956). However, the time-average equation applied to carbonate rocks must be used with caution (Wang, 1997). Robertson (1993) shows a positive correlation between the V_p/V_s ratio and the porosity for carbonate rocks with porosity $<10\%$. This trend is consistent with our observations (compare Tables 1 and 2), but this relation was not explicitly used because it was limited to porosities lower than those in our models. Anselmetti and Eberli (1997) provide direct relations between porosity (up to 60%) and both V_p and V_s from observations of Bahama and Maiela carbonates, with ages ranging from Late Jurassic to Pleistocene, that can be used to infer the diagenetic history.

Table 2 shows the porosity of the Parigi reservoir at each CMP location obtained with a variety of techniques using the seismic parameters estimated above. Higher porosities are consistently predicted at off-reef CMP locations 2, 5, and 6 compared to those of on-reef CMP locations 1, 3, and 4. Some predicted porosities exceed the critical porosity for carbonate of 40% (Nur et al., 1998), which can occur if the carbonate is vugular. Less consolidated carbonate sediment at the off-reef locations may also be the cause of these higher porosities. Also, the different depositional processes at the off-reef locations, in which the carbonate was deposited as sediment (by reef erosion) along with other clastic material, compared to those at the on-reef locations would decrease the purity of carbonate, in turn biasing the calculated porosities based on the pure carbonate assumption.

Porosities estimated independently of the AVA measurements (which include calculation from density and from the time-average equation) fall below Anselmetti and Eberli's (1997) predictions (Table 2). Underestimation of porosity by

Table 2. Porosity estimations from seismic parameters for each CMP location using different calculation techniques (Wyllie et al., 1956; Piggot et al., 1989, 1990; and Santoso et al., 1995; Anselmetti and Eberli, 1997). Upper and lower limits of the calculated porosities are produced by assuming pure limestone and dolomite. Densities for porosity calculations are obtained from the crossplot shown in Figure 5 and Gardner et al.'s (1974) equation.

Calculation method	Target porosity (%)					
	CMP 1	CMP 2	CMP 3	CMP 4	CMP 5	CMP 6
From crossplot density	13.0–21.0	27.0–33.5	21.0–27.0	22.5–29.0	30.0–34.5	31.5–37.5
From Gardner's density	14.0–21.5	23.0–29.5	18.0–25.5	21.0–27.0	24.5–31.0	26.0–32.0
Time average	23.5–27.5	33.5–37.0	28.0–32.0	30.0–33.0	33.5–39.0	37.0–40.0
Anselmetti and Eberli from V_p	25.4	39.4	31.7	34.0	42.2	44.2
Anselmetti and Eberli from V_s	17.7	36.7	26.0	30.7	30.8	40.9
Piggot (crossplot density)	25.1	48.0	34.1	39.6	44.0	54.0
Piggot (Gardner's density)	25.4	47.0	33.8	39.1	43.5	52.9

the time-average predictions is demonstrated by Anselmetti and Eberli (1997). However, estimations based on AVA analysis results (e.g., Santoso et al., 1995), using techniques derived by Piggot et al. (1990), show higher average porosities than Anselmetti and Eberli's predictions. This positive departure from the normal predicted V_p -porosity trend may be because of the predominant pore types of intraframe and moldic porosities, in which the high-porosity carbonate still maintains its high V_p because of the strength of the frame. Combined with the previously published Parigi porosity information (e.g., Yaman et al., 1991; Arianto, 1993), the average data values ($V_p \sim 2.8$ – 4.1 km/s; porosity ~ 25 – 54%) suggest that the diagenetic stage in the Parigi Formation could be interpreted being characterized by dissolution, where the porosities are dominantly moldic or intraframe (Anselmetti and Eberli, 1997).

Porosities ranging from 26% to 40% are estimated (Table 2) at the target reefs (at CMPs 1, 3, and 4). These results are consistent with the previous core data and the estimation of Parigi reef porosity by Santoso et al. (1995). There is no significant difference in the porosity estimates between CMPs 3 and 4 (Table 2), which is also reflected by their similar estimated V_p values (Table 1). However, as shown in Figures 7, 10, and 11, their AVA responses are very different, which is attributed to pore-fluid density difference (brine versus gas) and the overburden attenuation.

DISCUSSION AND SYNOPSIS

We have analyzed and simulated the AVA responses for six CMP locations over and around carbonate reefs in the Parigi Formation of the northwest Java basin. Although we have neglected some aspects that may affect the AVA (such as details of near-surface effects), the forward-modeling results provide a model consistent with brine saturation at all CMPs except CMP 4; the latter was modeled with low density in the Parigi and low Q in the overburden, consistent with gas saturation of both. The porosity estimations for the Parigi in Table 2 scatter widely between different calculation techniques. This indicates that porosity still cannot be determined solely from V_p , V_s , and density—even when the lithology is fairly well constrained.

Within a specific carbonate environment, the elastic properties depend mainly, but not exclusively, on the porosity. For example, D'Angelo et al. (1997) find this to be true from their laboratory measurements on chalk. However, Anselmetti and Eberli (1997) warn that the influence of pore type must also be included when attempting to predict velocity from porosity; they show that rocks with 40% to 50% porosity, moldic, or vugular pore structure can produce velocities that are a factor of two higher than those with interparticle or intercrystalline pores. They also show that V_s is more affected than V_p by high porosity. Marion and Jizba (1997) show an $\sim 10\%$ decrease in V_p associated with substituting gas for brine (at an unspecified porosity) at ultrasonic frequencies. This decrease is greater than that predicted by the Gassmann model for seismic frequencies, and this discrepancy increases at low porosity and high velocity. The discrepancy is explained if the effects of pore fluid in carbonates are similar to those in clastics, and it becomes more important as porosity increases. Our model results are consistent with these guiding concepts.

The off-reef CMPs are well fitted with models that are consistent with brine saturation and have negatively sloping AVA

curves. CMP 1 has a slight upturn (which may or may not be significant) at the higher incidence angles, which may indicate a minor hydrocarbon content. CMP 3 has an oil show in the Parigi in the well and a moderate positive AVA slope at the higher incidence angles. CMP 4 could only be approximated with gas saturation and has a strong positive AVA slope. Thus, it appears that the AVA slope can be used in this environment to indicate the presence of hydrocarbons.

The models (at all CMPs) are not necessarily unique; other models may predict the data equally well. However, the parameters in the current models are either estimated directly from the seismic data or well logs or are consistent with the empirical relations observed in similar environments elsewhere. The seismic parameters are also consistent with the geologic environment; this was particularly crucial for obtaining a plausible interpretation and prediction of the data at CMP 4.

At the anomalous CMP 4, the elastic AVA responses are controlled by three main factors. The first is the position of the critical P -wave reflection, which is determined by the contrast in V_p . The second is the near-offset reflectivity, which determines the density contrast at the top of the reservoir (since the V_p contrast is already constrained by the critical angle). The third is the slope of the AVA curve in the precritical region, whose reflectivity contribution is mainly controlled by the V_p/V_s ratio contrast and whose transmission contribution is mainly controlled by the attenuation in the overburden. The presence of a relatively high frame density and high porosity in the Parigi results in a significant decrease of the bulk density when a low-density gas substitutes for brine in the vugular pore space. This, combined with small critical angle at the sediment-carbonate interface and local high attenuation in the overburden around the reflection point of CMP 4, produces a probable hydrocarbon indicator as a strong positive AVA trend. This diagnostic has not been verified by drilling.

Although all three are over reefs, CMP 4 appears to be a better potential well location than CMPs 1 or 3. The AVA analysis and modeling results indicate that the extremely different AVA behavior of CMP 4 is probably the consequence of the presence of gas. This is also consistent with its position at the structural high of the reef. It is premature, on the basis of the results here, to suggest drilling at CMP 4 because only one seismic line has been considered. It is necessary to check for consistency of response at nearby locations to determine the volume of structural closure and to locate the actual structure high, which may be some distance off the present line. Nevertheless, we have provided a potentially useful diagnostic tool which, if it proves to be reliable, can be applied to search for targets in nearby reefs.

ACKNOWLEDGMENTS

The research leading to this paper was supported by Pertamina, Indonesia; by the Petroleum Research Fund of the American Chemical Society under grant 32721-AC2; and by the sponsors of the UT-Dallas Geophysical Consortium. The authors appreciate the help of D. Santoso in obtaining the field data from Pertamina for this study. Constructive comments by Gerard Schuster and two anonymous reviewers improved the paper and are much appreciated. This paper is Contribution 936 from the Geosciences Department at the University of Texas at Dallas.

REFERENCES

- Adriansyah and McMechan, G. A., 1998, Effect of attenuation and scattering on AVO measurement: *Geophysics*, **63**, 2025–2034.
- Alkhalifah, T., 1997, Velocity analysis using nonhyperbolic moveout in transversely isotropic media: *Geophysics*, **62**, 1839–1834.
- Allen, J. L., and Peddy, C. P., 1993, Amplitude variation with offset: Gulf Coast case studies: *Soc. Expl. Geophys.*
- Anselmetti, F. S., and Eberli, G. P., 1997, Sonic velocity in carbonate sediments and rocks, in Palaz, I., and Marfurt, K. J., Eds., *Carbonate seismology: Soc. Expl. Geophys.*, 53–74.
- Arianto, K., 1993, A model of extended hydrocarbon reservoir and the change of finding traps in carbonate build up, offshore N.W. Java: 18th Ann. Conv., Indonesian Assoc. Geophys., Proceedings, 103–110.
- Burbury, J. E., 1977, Seismic expression of carbonate build ups north-west Java basin: 6th Ann. Conv., Indonesian Petr. Assoc., Proceedings, 239–267.
- Castagna, J. P., Batzle, M. L., and Kan, T. K., 1993, Rock physics—The link between rock properties and AVO response, in Castagna, J. P., and Backus, M. M., Eds., *Offset dependent reflectivity: Theory and practice of AVO analysis: Soc. Expl. Geophys.*, 135–171.
- Chacko, S., 1989, Porosity identification using amplitude variation with offset: Examples from south Sumatra: *Geophysics*, **54**, 942–951.
- Chiburis, E. F., 1984, Analysis of amplitude versus offset to detect gas/oil contacts in the Arabian Gulf: 54th Ann. Internat. Mtg., Soc. Expl. Geophys., Expanded Abstracts, 669–670.
- , 1987, Studies of amplitude versus offset in Saudi Arabia: 57th Ann. Internat. Mtg., Soc. Expl. Geophys., Expanded Abstracts, 614–616.
- , 1993, AVO applications in Saudi Arabia, in Castagna, J. P., and Backus, M. M., Eds., *Offset dependent reflectivity: Theory and practice of AVO analysis: Soc. Expl. Geophys.*, 211–229.
- D'Angelo, R. M., Brandal, M. K., and Rørvik, K. O., 1997, Porosity detection and mapping in a basinal carbonate setting, offshore Norway, in Palaz, I., and Marfurt, K. J., Eds., *Carbonate seismology: Soc. Expl. Geophys.*, 321–336.
- Dey-Sarkar, S. K., and Svatek, S. V., 1993, Prestack analysis—An integrated approach for seismic interpretation in clastic basins, in Castagna, J. P., and Backus, M. M., Eds., *Offset dependent reflectivity: Theory and practice of AVO analysis: Soc. Expl. Geophys.*, 57–77.
- Domenico, S. N., 1984, Rock lithology and porosity determination from shear and compressional wave velocity: *Geophysics*, **49**, 1188–1195.
- , 1993, Sandstone and limestone porosity determination from shear and compressional wave velocity: 63th Ann. Internat. Mtg., Soc. Expl. Geophys., Expanded Abstracts, 353–355.
- Estill, R., and Wroldstad, K., 1993, Interpretive aspects of AVO—Application to offshore Gulf Coast bright-spot analysis, in Castagna, J. P., and Backus, M. M., Eds., *Offset dependent reflectivity: Theory and practice of AVO analysis: Soc. Expl. Geophys.*, 267–284.
- Gardner, G. H. F., Gardner, L. W., and Gregory, A. R., 1974, Formation velocity and density—The diagnostic basics for stratigraphic traps: *Geophysics*, **39**, 770–780.
- Gregory, A. R., 1976, Fluid saturation effects on dynamic elastic properties of sedimentary rocks: *Geophysics*, **41**, 895–913.
- Hake, H., Helbig, K., and Mesdag, C. S., 1984, Three term Taylor series for t^2 - x^2 curves over layered transversely isotropic ground: *Geophys. Prosp.*, **32**, 828–850.
- Hall, D. J., Adamick, J. A., Skoyles, D., DeWildt, J., and Erickson, J., 1995, AVO as an exploration tool: Gulf of Mexico case studies and examples: *The Leading Edge*, **14**, 863–868.
- Hamilton, W., 1976, Tectonics of the Indonesian region: U.S. Geological Survey Prof. Paper 1078.
- Ho, M. S., Lee, S. S., and Purnell, G. W., 1992, Comparison of P -wave AVO techniques for locating zones of fractured dolomite within non-reservoir limestone: 62nd Ann. Internat. Mtg., Soc. Expl. Geophys., Expanded Abstracts, 867–869.
- Juhlin, C., and Young, R., 1993, Implications of thin layers for amplitude variation with offset (AVO) studies: *Geophysics*, **58**, 1200–1204.
- Kim, K. Y., Wroldstad, K. H., and Aminzadeh, F., 1993, Effects of transverse isotropy on P -wave AVO for gas sands: *Geophysics*, **58**, 883–888.
- Klimentos, T., 1995, Attenuation of P - and S -waves as a method of distinguishing gas and condensate from oil and water: *Geophysics*, **60**, 447–458.
- Koefoed, O., 1955, On the effect of Poisson's ratios of rock strata on the reflection coefficients of plane waves: *Geophys. Prosp.*, **3**, 381–387.
- Landrø, M., Buland, A., and D'Angelo, R., 1995, Target-oriented AVO inversion from Valhall and Hod fields: *The Leading Edge*, **14**, 855–861.
- Lu, H. X., and Lines, L., 1995, AVO and Devonian reef exploration: Difficulties and possibilities: *The Leading Edge*, **14**, 879–881.
- Marion, D., and Jizba, D., 1997, Acoustic properties of carbonate rocks: Use in quantitative interpretation of sonic and seismic measurements, in Palaz, I., and Marfurt, K. J., Eds., *Carbonate seismology: Soc. Expl. Geophys.*, 75–93.
- Martinez, R. D., 1993, Wave propagation effects on amplitude variation with offset measurements: A modeling study: *Geophysics*, **58**, 534–543.
- Martinez, R. D., and McMechan, G. A., 1991, τ - p seismic data for viscoelastic media—Part 1: Modeling: *Geophys. Prosp.*, **39**, 141–156.
- Nur, A., Mavko, G., Dvorkin, J., and Galmudi, D., 1998, Critical porosity: A key to relating physical properties to porosity in rocks: *The Leading Edge*, **17**, 357–362.
- Ostrander, W. J., 1984, Plane-wave reflection coefficients for gas sands at nonnormal angles of incident: *Geophysics*, **49**, 1637–1648.
- Patmosukismo, S., and Yahya, I., 1974, The basement configuration of the northwest Java area: 3rd Ann. Conv., Indonesian Petr. Assoc., Proceedings, 129–152.
- Pickett, G. R., 1963, Acoustic character logs and their applications in formation evaluation: *J. Petr. Tech.*, **15**, 659–667.
- Piggot, J. D., Shrestha, R. K., and Warwick, R. A., 1989, Young's modulus from AVO inversion: 59th Ann. Internat. Mtg., Soc. Expl. Geophys., Expanded Abstracts, 832–835.
- , 1990, Direct determination of carbonate reservoir porosity and pressure from AVO inversion: 60th Ann. Internat. Mtg., Soc. Expl. Geophys., Expanded Abstracts, 1533–1536.
- Reminton, C. H., and Pranyoto, U., 1985, A hydrocarbon generation analysis in northwest Java basin using Lopatin's method: 14th Ann. Conv., Indonesian Petr. Assoc., Proceedings, 121–141.
- Richards, T. C., 1961, Motion of the ground on arrival of reflected longitudinal and transverse waves at wide-angle reflection distances: *Geophysics*, **24**, 277–297.
- Robertson, J. D., 1993, Carbonate porosity from S/P traveltime ratio: 63rd Ann. Internat. Mtg., Soc. Expl. Geophys., Expanded Abstracts, 356–358.
- Rutherford, S. R., and Williams, H. R., 1989, Amplitude-versus-offset variations in gas sands: *Geophysics*, **54**, 680–688.
- Samec, P., and Blangy, J. P., 1992, Viscoelastic attenuation, anisotropy and AVO: *Geophysics*, **57**, 441–450.
- Santoso, D., Alfian, Alam, S., Sulistiyono, Hendrajaya, L., and Munadi, S., 1995, Estimation of limestone reservoir porosity by seismic attribute and AVO analysis: *Expl. Geophys.*, **26**, 437–443.
- Schlumberger, 1984, Log interpretation charts: Schlumberger Ltd. Publ. SMP-7006.
- Shuey, R. T., 1985, A simplification of the Zoeppritz equations: *Geophysics*, **50**, 609–614.
- Snyder, A. G., and Wroldstad, K. H., 1992, Direct detection using AVO, Central Graben, North Sea: *Geophysics*, **57**, 313–325.
- Wang, Z., 1997, Seismic properties of carbonate rocks, in Palaz, I., and Marfurt, K. J., Eds., *Carbonate seismology: Soc. Expl. Geophys.*, 29–52.
- Widmaier, M. T., Shapiro, S. A., and Hubral, P., 1996, AVO correction for scalar waves in the case of a thinly layered reflector overburden: *Geophysics*, **61**, 520–528.
- Wight, A., and Hardian, D., 1982, Importance of diagenesis in carbonate exploration and production, lower Baturaja Carbonates, Krishna field, Java Sea: 11th Ann. Conv., Indonesian Petr. Assoc., Proceedings, 211–235.
- Wyllie, M. R. J., Gregory, A. R., and Gardner, L. W., 1956, Elastic wave velocities in heterogeneous and porous media: *Geophysics*, **21**, 41–70.
- Xu, Y., Gardner, G. H. F., and McDonald, J. A., 1993, Some effects of velocity variation on AVO and its interpretation: *Geophysics*, **58**, 1297–1300.
- Yaman, F., Ambismar, T., and Bukhari, T., 1991, Gas exploration in Parigi and pre-Parigi carbonate buildups, NW Java Sea: 20th Ann. Conv., Indonesian Petr. Assoc., Proceedings, 319–346.
- Zoeppritz, K., 1919, Über Erdbebenwellen VII B, Über reflexion und durchgang seismischer Wellen durch Unstetigkeitsflächen: *Gottinger Nachr.*, **K1**, 66–84.